



Bioinspired tactile perception platform with information encryption function

Zhi-Wen Shi(石智文), Zheng-Yu Ren(任征宇), Wei-Sheng Wang(王伟胜), Hui Xiao(肖惠), Yu-Heng Zeng(曾俞衡), and Li-Qiang Zhu(竺立强)

Citation: Chin. Phys. B, 2022, 31 (9): 098506. DOI: 10.1088/1674-1056/ac7a15

Journal homepage: <http://cpb.iphy.ac.cn>; <http://iopscience.iop.org/cpb>

What follows is a list of articles you may be interested in

Quantum oscillations in a hexagonal boron nitride-supported single crystalline InSb nanosheet

Li Zhang(张力), Dong Pan(潘东), Yuanjie Chen(陈元杰), Jianhua Zhao(赵建华), and Hongqi Xu(徐洪起)
Chin. Phys. B, 2022, 31 (9): 098507. DOI: 10.1088/1674-1056/ac7455

Implementation of an 8-bit bit-slice AES S-box with rapid single flux quantum circuits

Ruo-Ting Yang(杨若婷), Xin-Yi Xue(薛新伊), Shu-Cheng Yang(杨树澄), Xiao-Ping Gao(高小平), Jie Ren(任洁), Wei Yan(严伟), and Zhen Wang(王镇)
Chin. Phys. B, 2022, 31 (9): 098501. DOI: 10.1088/1674-1056/ac70b9

Wake-up effect in $\text{Hf}_{0.4}\text{Zr}_{0.6}\text{O}_2$ ferroelectric thin-film capacitors under a cycling electric field

Yilin Li(李屹林), Hui Zhu(朱慧), Rui Li(李锐), Jie Liu(柳杰), Jinjuan Xiang(项金娟), Na Xie(解娜), Zeng Huang(黄增), Zhixuan Fang(方志轩), Xing Liu(刘行), and Lixing Zhou(周丽星)
Chin. Phys. B, 2022, 31 (8): 088502. DOI: 10.1088/1674-1056/ac5977

Characterization of topological phase of superlattices in superconducting circuits

Jianfei Chen(陈健菲), Chaohua Wu(吴超华), Jingtao Fan(樊景涛), and Gang Chen(陈刚)
Chin. Phys. B, 2022, 31 (8): 088501. DOI: 10.1088/1674-1056/ac5612

Microstructural, magnetic and dielectric performance of rare earth ion (Sm^{3+})-doped MgCd ferrites

Dandan Wen(文丹丹), Xia Chen(陈霞), Dasen Luo(骆大森), Yi Lu(卢毅), Yixin Chen(陈一鑫), Renpu Li(黎人溥), and Wei Cui(崔巍)
Chin. Phys. B, 2022, 31 (7): 078503. DOI: 10.1088/1674-1056/ac398c

Bioinspired tactile perception platform with information encryption function

Zhi-Wen Shi(石智文)^{1,2}, Zheng-Yu Ren(任征宇)², Wei-Sheng Wang(王伟胜)^{1,2}, Hui Xiao(肖惠)², Yu-Heng Zeng(曾俞衡)², and Li-Qiang Zhu(竺立强)^{1,2,†}

¹School of Physical Science and Technology, Ningbo University, Ningbo 315211, China

²Ningbo Institute of Materials Technology and Engineering, Chinese Academy of Sciences, Ningbo 315201, China

(Received 20 April 2022; revised manuscript received 28 May 2022; accepted manuscript online 18 June 2022)

Mimicking tactile perception is critical to the development of advanced interactive neuromorphic platforms. Inspired by cutaneous perceptual functions, a bionic tactile perceptual platform is proposed. PDMS-based tactile sensors act as bionic skin touch receptors. Flexible indium tin oxide neuromorphic transistors fabricated with a single-step mask processing act as artificial synapses. Thus, the tactile perceptual platform possesses the ability of information processing. Interestingly, the flexible tactile perception platform can find applications in information encryption and decryption. With adoption of cipher, signal transmitted by the perception platform is encrypted. Thus, the security of information transmission is effectively improved. The flexible tactile perceptual platform would have potentials in cognitive wearable devices, advanced human-machine interaction system, and intelligent bionic robots.

Keywords: flexible oxide neuromorphic transistor, tactile perception platform, information encryption

PACS: 85.30.Tv

DOI: 10.1088/1674-1056/ac7a15

1. Introduction

Because of the limitations of conventional von Neumann architecture in big data processing, including high energy consumption and large size, it is highly desirable to develop candidate computing strategy. Thus, brain inspired artificial intelligence (AI) technology has attracted great attention.^[1] It would deal with complex non-structural cognitive tasks, including learning, memory, decision-making and reasoning, *etc.*^[2,3] With continuous upgrading and innovation of information technology, AI is getting penetrated into all aspects of daily life, including healthcare services, autonomous driving, manufacturing, finance, personalized online education systems, *etc.*^[4-7] Research indicates that brain's superior data processing function mainly comes from synaptic plasticity and neural computation in nervous system with the integrated storage and computing architecture.^[8] Therefore, adoption of neuromorphic devices is considered to be a promising approach in hardware based AI.^[9,10] Up to date, several kinds of neuromorphic devices have been proposed, including two-terminal resistance switchable devices^[11-13] and three-terminal transistors.^[14-17] Except for basic bionic synaptic responses, advanced neural algorithms have also been realized on neuromorphic devices, including pattern recognition,^[18,19] sparse coding,^[20] learning rules,^[21,22] *etc.*

Interestingly, brain multisensory system integrates five major sense organs, including tactile sensation, visual sensation, auditory sensation, olfactory sensation and gustatory sensation. These perceptual activities enable us to adapt to

external environment and to deal with practical interactive issues.^[23-25] As shown in the top panel of Fig. 1(a), for biological cutaneous afferent nerves, external pressure loaded on the skin changes the potentials of receptors embedded within skin. Cell bodies of sensory neurons integrate potentials and activate action potentials with coded pressure information. Thus, axons transfer action potentials to central nervous system (CNS) through intermediate neurons. While CNS processes pressure information by integrating action potentials from multiple synapses.^[26] Inspired by the brain multisensory system, artificial perception learning systems could be proposed by integration of information receiving unit and information processing unit. Fortunately, various sensors have been proposed, including pressure sensors,^[27,28] piezoelectric capacitance sensors,^[29] photoelectric sensors,^[30] gas sensors,^[31,32] *etc.* Especially with the increasing demands of wearable electronics, these sensors have also been designed for electronics skin (E-skin) applications.^[33-36] Recently, inspired by body multiorgan perceive learning, flexible neuromorphic systems with integrated sensors have been shown to perceive and process various sensory information.^[26,37-41] Such flexible artificial perception learning system would endow new intention for human-machine interface, robotics, and prosthetics.^[42,43] Moreover, hybrid sensor networks with biological afferent features are expected to solve complex practical problems, including image parsing, facial feature recognition, adaptive control, *etc.* Thus, artificial perception platform would let the portable system possess multi-modal perception functions with advanced intelligence.

[†]Corresponding author. E-mail: zhuliqiang@nbu.edu.cn or lqzhu@nimte.ac.cn

Unfortunately, information sensed by sensors can be easily obtained illegally during transmission in artificial perception system. Therefore, information encryption strategy needs to be developed to ensure the security of information transmission. Here, a flexible tactile perception platform is proposed for information encoding and encryption applications, as schematically shown in the lower panel of Fig. 1(a). An

XNOR logic circuit is used to encrypt the tactile perceptual signals. Thus, information transmitted in the whole perception platform is the encrypted information, which avoids the illegal acquisition of tactile signals. Moreover, the signals can also be decrypted using XNOR logic circuits. The proposed system would have potentials in congenitive wearable devices and advanced human-machine interaction system.

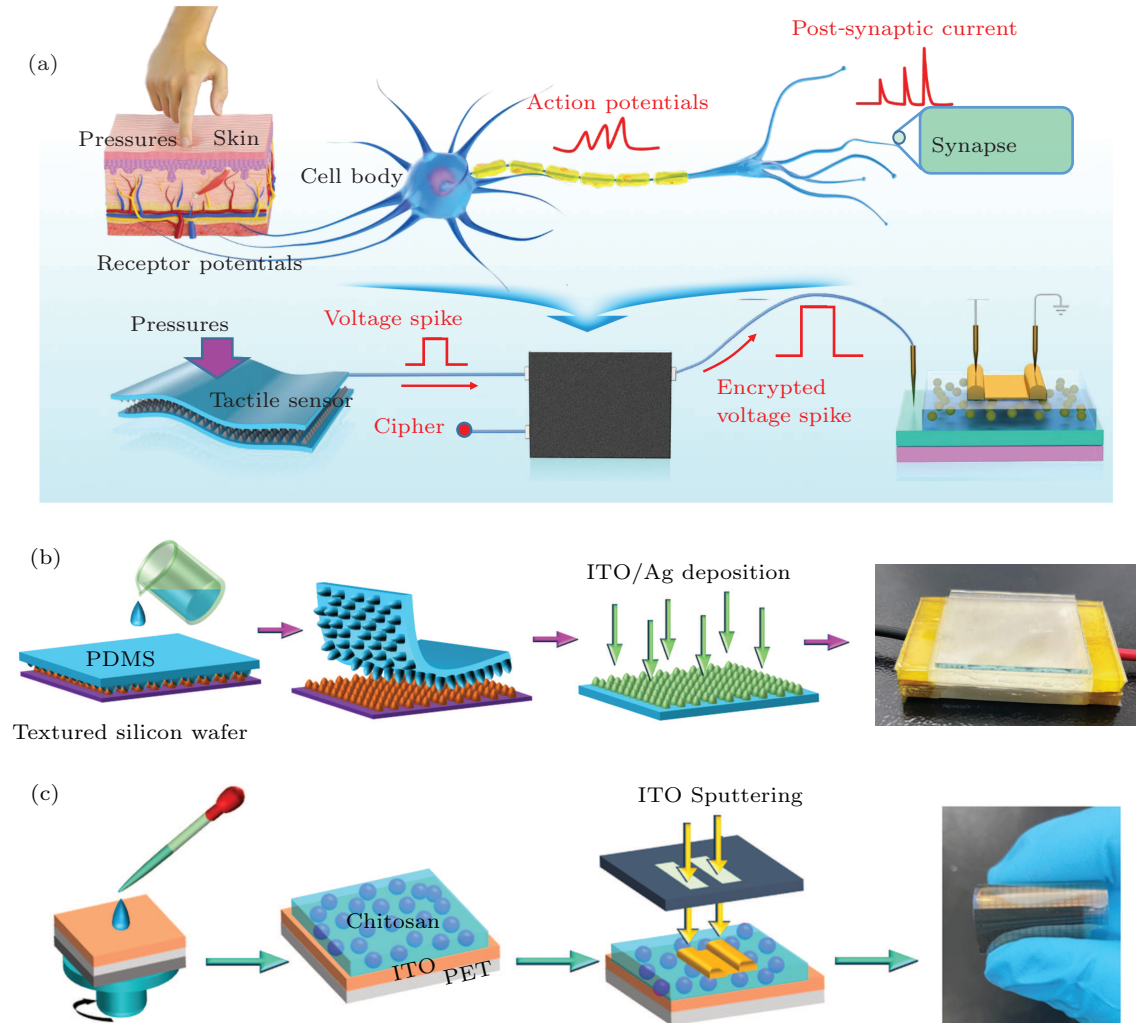


Fig. 1. (a) Schematic diagram of simplified biological cutaneous afferent nerves and the proposed flexible tactile perception platform for information encryption applications. (b) Schematic diagram of the fabrication of tactile sensor. (c) Schematic diagram of the fabrication of ITO neuromorphic transistor.

2. Experimental details

2.1. Fabrication of tactile sensors

Firstly, tactile sensor is fabricated with solution processing by using KOH solution etched textured silicon wafer as mold, as schematically shown in Fig. 1(b). The detail processing could be found in Ref. [44]. With the textured silicon wafer, random flipped pyramid structure can be copied onto the surface of the PDMS elastomer. Then, Ag/ITO double conductive layer was deposited on the PDMS elastomer. Finally, two Ag/ITO/PDMS membrane with size of $4\text{ cm} \times 2.5\text{ cm}$ were encapsulated with Kapton tape to construct a pressure sensor with two membranes separated for $\sim 0.8\text{ mm}$. It acts as a tac-

tile receptor for tactile perception platform applications.

2.2. Fabrication of flexible oxide neuromorphic transistors

Environmentally friendly oxide neuromorphic transistors were fabricated with a low cost processing, as schematically shown in Fig. 1(c). Here, chitosan-based electrolyte is used as gate dielectrics. It has several priorities. Firstly, it is a kind of bio-material and could be obtained easily from nature with low cost. Secondly, chitosan-based electrolyte film could be prepared with a low-cost solution processing. With protonation process activated by acetic acid, amino groups will be produced within chitosan. Therefore, the chitosan film could

exhibit high proton conductivity. Thus, low operation voltage is expected for the chitosan gated transistor, which is of interests for neuromorphic electronic applications. Additionally, as a kind of green polymer material, chitosan has characteristics of non-toxicity and good biocompatibility. Thus, it could have potentials in the field of green neuromorphic system. Firstly, 2-wt% chitosan and 2-wt% acetic acid were dissolved in 96-wt% deionized water at room temperature. After standing for 24 hours, chitosan solution was coated on conductive polyethylene terephthalate (PET) substrate by dip-coating processing. It was then put into a drying oven at 35 °C and 45 °C for 6 hours each to form chitosan based electrolyte film. Then, ITO source and drain electrodes with thickness of ~ 100 nm were sputtered onto the chitosan film patterned using a metal shadow mask in pure Ar environment. The sputtering pressure, Ar flow rate and sputtering power were set to 0.5 Pa, 14 SCCM, and 100 W, respectively. The sputtering rate is ~ 7 nm/min. Due to the reflection of nanoparticles at the mask edge, ITO channel layer can be formed between source and drain electrodes. Thus, an ITO neuromorphic transistor with a bottom gate configuration was obtained.

2.3. Characterization and electrical measurements

Microstructure of PDMS elastomer and Ag/ITO/PDMS films was characterized by field emission scanning electron microscopy (Verios G4 UC). Frequency dependence capacitance and impedance spectra of chitosan-based electrolyte were characterized by Solartron 1260A impedance analyzer. Electrical performances of tactile sensors, neuromorphic transistors and artificial tactile perception platform were characterized using Keithley 4200 SCS semiconductor parameter analyzer. All the electrical properties were characterized at room temperature with an air relative humidity of $\sim 55\%$.

3. Results and discussion

Sensory activities of human beings require synergetic cooperation of receptors, afferent nerves and neural circuit.^[45] Skin is an important organ that receives external pressure stimuli. It senses external stimulation signals and converts them into electrical signals, which are then transmitted to specific neural circuit in CNS through afferent nerves. Specific neural circuit will process information and will trigger tactile perception. Inspired by the sensory activities of biological skin, we propose a low-cost method to fabricate tactile pressure sensors that could convert external pressure signals into electrical signals. Figure 2(a) shows the top-view SEM image of a textured silicon mold with random pyramid microstructure. The lower inset in Fig. 2(a) shows the top-view SEM image of PDMS film. Random flipped pyramid structure is observed on the PDMS surface. The Top inset in Fig. 2(a) shows the

top-view SEM image of Ag/ITO/PDMS conductive flexible membrane. Peaks and valleys can be clearly observed. Such structure helps good sensory performances for tactile device. Figure 2(b) schematically shows the tactile sensor with and without pressure. Under external pressure, the resistance of the sensor will decrease because of the point or surface contact. Thus, the pressure stimuli will be converted into electrical signals if the tactile sensor is biased at a certain voltage. When testing electrical performances of the pressure sensor, a 2.5 cm \times 2.5 cm glass plate was placed on the sensor to ensure that the force on the sensor was as uniform as possible. The mass of the glass plate is 1.75 g. External sweep biases ranged between -0.3 V and 0.3 V were applied to measure the conductances of the sensor at different pressures. The conductances were shown in Fig. 2(c). When pressure increases from 0.34 kPa to 4.82 kPa, the conductance increases from 0.16 S to 0.31 S. When pressure is loaded, the two conductive layers are extruded, which induces increased conductance. At the beginning, the changes in the degree of extrusion is significant at low pressure. While the changes in the degree of extrusion is getting less significant at increased pressure. Thus, the changes in conductance is significant at low pressure. While it is getting less significant at increased pressure. We have also applied five identical continuous pressure stimuli with a duration time of 1.3 s on the sensor biased at a constant voltage of 0.2 V. Figure 2(d) shows the current responses. Peak currents are observed to be relatively stable at the same pressure stimuli. When the pressure is ~ 0.66 kPa, peak current is ~ 32.5 mA. When the pressure is ~ 1.62 kPa, peak current increases to ~ 47.3 mA. When the pressure is ~ 4.82 kPa, peak current increases further to ~ 60.1 mA. Figure 2(e) shows current responses of the sensor at a constant bias of 0.2 V through repeated loading and unloading pressure stimuli of 0.34 kPa with a frequency of ~ 0.7 Hz. It can be seen that the sensor shows good repeatabilities and durabilities, indicating that the proposed sensor could be used as a tactile receptor to imitate tactile perception activities.

Figure 3(a) shows output characteristics of the ITO neuromorphic transistor, indicating typical N-type performances with good Ohmic contact. Good stability against external mechanical bending stress is a prerequisite for flexible electronics. We tested electrical performances of flexible neuromorphic transistors against mechanical stress using a cyclic bending machine that can introduce repeated bending stresses. The bending rate is set at 480 r/min. The transistors were periodically bent with a bending radius of 3.0 cm. In every 1000 bends, the transistor is placed on a flat platform to measure transfer curve. Figure 3(b) shows the transfer curves. No observable shifts were obtained after receiving repeated bending stresses. Figure 3(c) shows corresponding electrical parameters. It can be seen that the electrical parameters are quite

stable. Threshold voltage (V_{th}), subthreshold swing and field-effect mobility are estimated to be -0.2 V, ~ 84 mV \cdot dec $^{-1}$, and ~ 18.7 cm 2 \cdot V $^{-1}$ \cdot S $^{-1}$, respectively. We have also taken transfer curves under different bending radii. It is observed

that the transfer curves remain stable under different bending stress (not shown here). Figure 3(d) shows the extracted electrical parameters as a function of bending radii. It is also observed that the electrical parameters are quite stable.

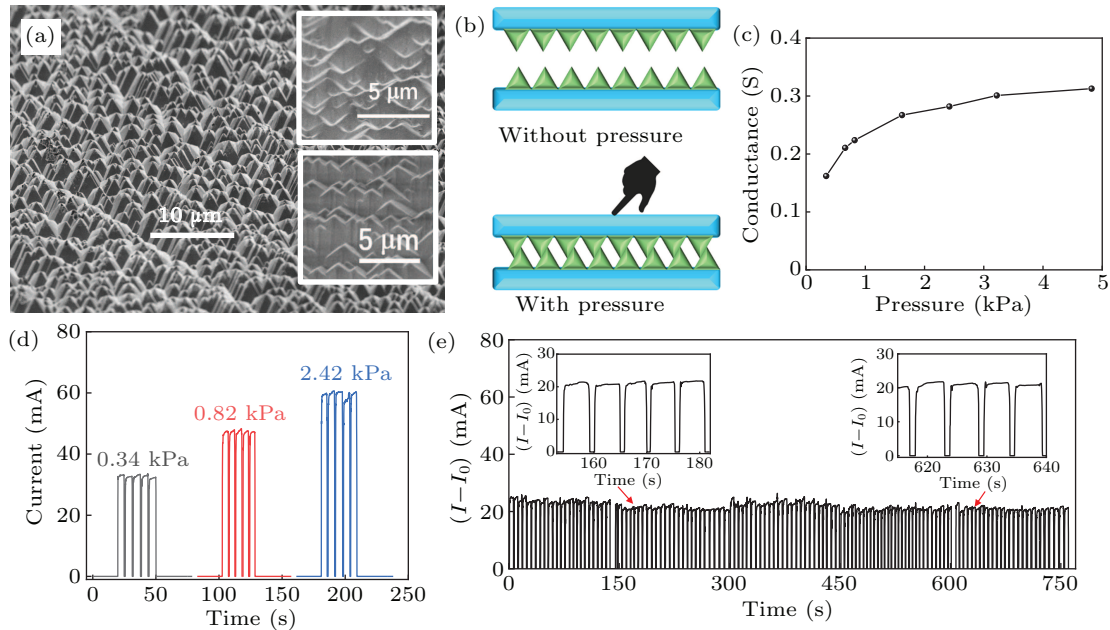


Fig. 2. (a) Top view SEM image of textured silicon mold. Lower inset: Top-view SEM image of the PDMS film. Top inset: Top-view SEM image of Ag/ITO/PDMS conductive flexible membrane. (b) Working principle of the tactile sensor. (c) Conductance of the sensor under loading different pressures. (d) Current responses of the tactile sensor under dynamic pressures with different intensities. (e) Dynamic current responses under repeated loading and unloading pressure stimuli of 0.34 kPa.

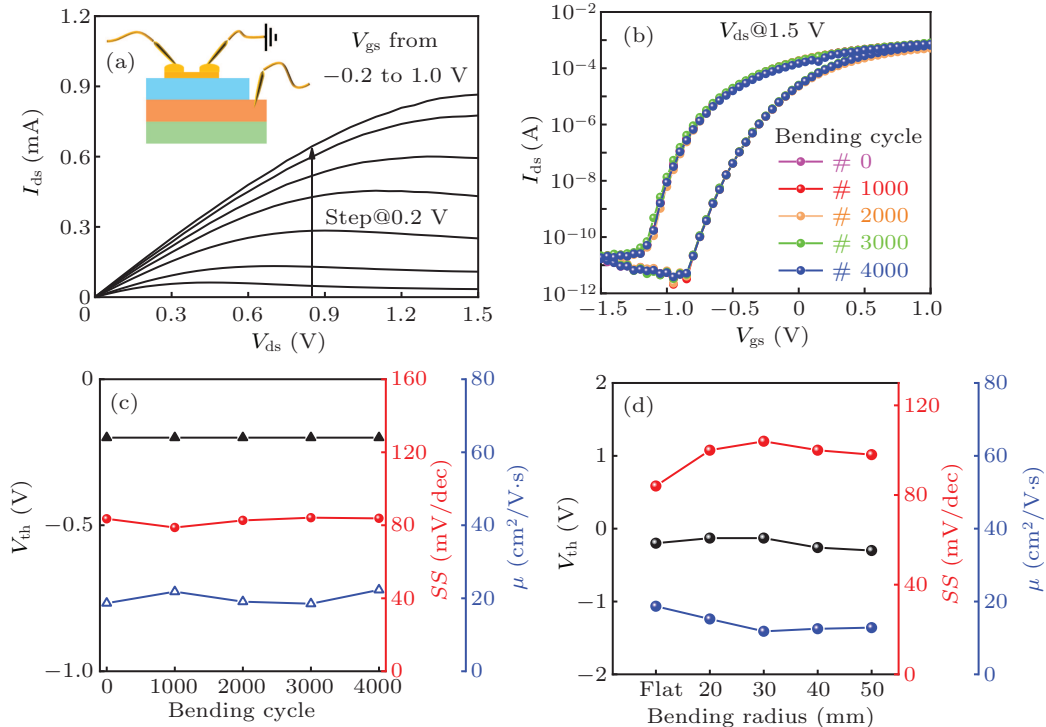


Fig. 3. (a) Output curves of chitosan-gated ITO neuromorphic transistors. Inset: the device configuration. (b) Transfer curves after loading different bending periods. (c) Extracted electrical parameters from panel (b). (d) Electrical parameters as a function of bending radii.

At the same time, two basic synaptic functions have also been demonstrated, including excitatory postsynaptic current (EPSC) and paired pulse facilitation (PPF). Post synaptic current is read out at a constant V_{ds} of 0.5 V. Figure 4(a) shows a

typical EPSC response triggered by a presynaptic spike of 1 V in amplitude and 20 ms in duration time. When paired presynaptic spikes arrive, paired EPSC responses will also be triggered. Inset in Fig. 4(b) presents a typical EPSC response for

spike interval time of 10 ms and spike duration time of 10 ms. The first absolute EPSC value (A_1) and the second absolute EPSC value (A_2) are estimated to be $\sim 0.9 \mu\text{A}$ and $\sim 1.4 \mu\text{A}$, respectively. Thus, PPF index, defined as $A_2/A_1 \times 100\%$, is $\sim 145\%$. With the increased interval time, the PPF index decreases gradually to $\sim 100\%$, as shown in Fig. 4(b). Furthermore, 50 presynaptic spikes with different amplitudes have also been loaded. It is found that peak EPSC values increase correspondingly, as shown in Fig. 4(c). When the spike amplitude is ranged between 1 V and 3 V, the EPSC will return back rapidly. In 0.5 s, 1.0 s, and 2.4 s after the spike ends, the EPSC value will return back to $10 \mu\text{A}$ for spikes with ampli-

tudes of 1 V, 2 V, and 3 V, respectively. While the EPSC values return back much slowly for high spike amplitudes. In 7.7 s, 15.9 s, and 22.9 s after the spike ends, the EPSC values will return back to $10 \mu\text{A}$ for spikes with amplitudes of 4 V, 5 V, and 6 V, respectively. Thus, synaptic weights show volatile activities for spike amplitudes ranged between 1 V and 3 V. While when the spike amplitude is higher, the EPSC gradually demonstrates non-volatile activities. For example, when the spike amplitude is 6 V, the EPSC will not returned back to the initial resting current. The behaviors indicate the transition from short-term plasticity (STP) to long-term-plasticity (LTP).

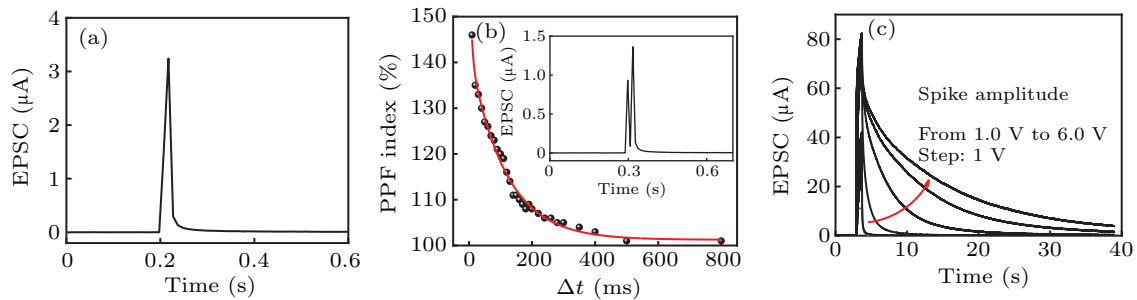


Fig. 4. (a) Typical EPSC response of flexible ITO neuromorphic transistor. (b) PPF index as a function of spike interval time (Δt). (c) Transition from STP to LTP mimicked on the flexible ITO synaptic transistor.

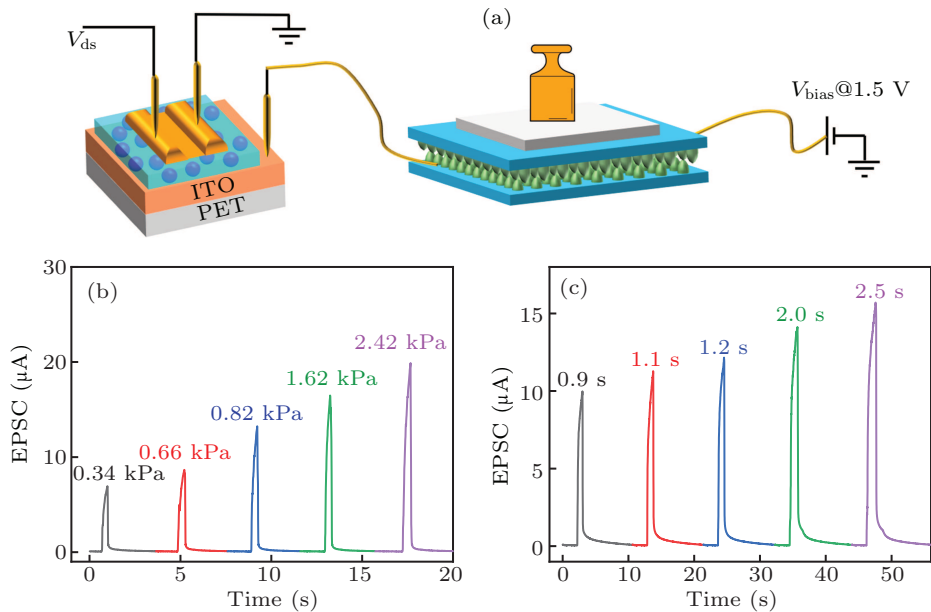


Fig. 5. (a) Schematic diagram of the tactile perception platform. (b) EPSC responses triggered with pressure spikes with duration time of 0.4 s. The pressure intensity increases from 0.34 kPa to 2.42 kPa. (c) Pressure duration-dependent EPSC responses with pressure intensity of 0.66 kPa.

Here, a flexible tactile perception platform is constructed by connecting the tactile sensor with the flexible chitosan gated ITO neuromorphic transistor. Figure 5(a) schematically shows the system. The tactile sensor is biased at 1.5 V. The two Ag/ITO/PDMS membranes of the tactile sensor are separated with tape to avoid continuous voltage loading on the gate. When a pressure is loaded on the sensor, the two membranes will contact with each other. Thus, the bias will load onto the gate of the neuromorphic transistor to modulate channel conductances. Figure 5(b) shows typical EPSC responses of the oxide neuromorphic transistor with a constant V_{ds} of 0.5 V under the loading of pressure spikes with duration time of 0.4 s. When the pressure is 2.42 kPa, peak EPSC current is $\sim 19.9 \mu\text{A}$. With the decreased pressures, peak EPSC values decrease correspondingly. When the pressure is 0.34 kPa, peak EPSC value is only $\sim 6.9 \mu\text{A}$. It should be noted here that the EPSC current will gradually decrease to a resting value of $\sim 0.2 \mu\text{A}$ when the loaded pressure is released. The behaviors are related to the STP. Furthermore, pressure

duration time will also affect EPSC responses, as shown in Fig. 5(c). The pressure intensity is 0.66 kPa. With the increase pressure duration time from 0.9 s to 2.5 s, peak EPSC values increase from 9.9 μ A to 15.7 μ A, correspondingly. The results indicate the high potential of the flexible tactile perception platform in humanoid intelligent robots and human–computer interface.

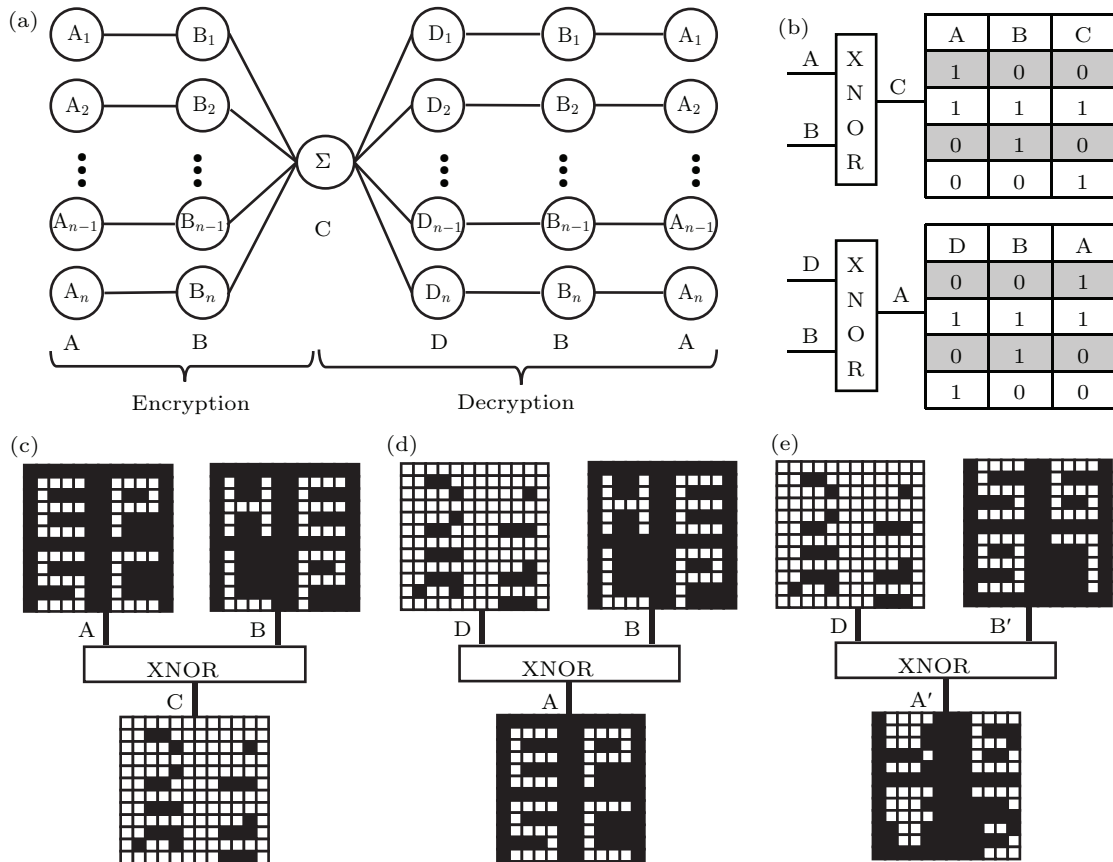


Fig. 6. (a) Flow chart of encryption and decryption functions for the proposed bionic perception system. (b) Truth table of XNOR operation. (c) Schematic diagram of encryption of information detected by 12×12 sensor arrays with encryption cipher “HELP” (B). (d) Schematic diagram of decryption process using the right decryption cipher “HELP” (B). (e) Decryption process using incorrect cipher “5697”.

Interestingly, information encryption and decryption function can be demonstrated on the tactile perception platform. Firstly, a 12×12 sensor array is suggested with each sensor connected to an oxide neuromorphic transistor. Thus, an EPSC response can be triggered when one of the 144 receptors detects a pressure stimulus. In this way, the handwritten content can be recognized by the architecture. When a receptor experiences a pressure stimulus, we code this state as “1”. Meanwhile, the transistor with an EPSC response can be encoded as “1”. On the contrary, when there is no external stimulus, EPSC response will not be triggered on the oxide neuromorphic transistor. Thus, the sensor can be coded as “0”. Correspondingly, the neuromorphic transistor can be encoded as “0”, too. It should be noted that human-like tactile sensing and information processing will be important for future intelligent human–computer interaction system. Moreover, the security of the perceived information in various bionic perception systems is particularly important for transmission process. However, the limitation of the bionic perception system is the illegal acquisition of the states. Here, an XNOR logic circuit is suggested to encode and encrypt the tactile perceptual signals.

The lower panel of Fig. 1(a) schematically shows the bionic perception system with encryption functions. Doing so, information transmitted in the whole sensory platform is the encrypted information. Figure 6(a) schematically shows the flow chart of the encryption and decryption function for the proposed bionic perception system. Figure 6(b) shows the truth table of XNOR operation. Top left panel in Fig. 6(c) schematically shows a handwritten information “EPSC” on the sensor array. The dark color pixel represents the state “0”, while the white color pixel represents the state “1”. We take the information detected by the sensor array as input (A). At the same time, a 12×12 cipher “HELP” was loaded into the XNOR logic circuit as input (B). The dark color pixel is the state “0” with a bias of 0 V, and the white color pixel is the state “1” with a bias of 1.5 V, as schematically shown in top right panel in Fig. 6(c). Output terminal C can output an encrypted information, as shown in the lower panel in Fig. 6(c). It could be observed that the encrypted information is no longer accurately recognized. Such encrypted signal is then loaded onto neuromorphic transistor. The white pixel in the lower panel in Fig. 6(c) is expressed with a spike with amplitude of 1.5 V

and a duration of 100 ms (state “1”), which causes an EPSC response in the transistor. While the dark pixel is expressed as 0 V (state “0”), which can’t cause an EPSC response. For decryption, information detected by the sensor is extracted and decrypted according to the channel state of the neuromorphic transistor arrays using XNOR circuit. When the neuromorphic transistor has an EPSC response (state “1”), it can be set to an input voltage spike (1.5 V, 100 ms) at another XNOR decryption circuit. Similarly, when neuromorphic transistor has no EPSC response (state “0”), no voltage spike is input in the XNOR decryption circuit. The encryption cipher “HELP” (B) was also input in the XNOR circuit. The information decrypted by the logic circuit is projected into 12×12 array. Figure 6(d) shows the decrypted information. It is found that the decrypted information is consistent with the original information. We have also loaded error decryption cipher with “5697” (B’), as shown in Fig. 6(e). It is found that the decrypted information (A’) is inconsistent with the original information (A). The results indicate that the original information can be decrypted only when the decryption cipher is consistent with the encryption cipher. This strategy can effectively avoid illegal acquisition of sensitive information during the transmission process in bionic perception system.

4. Conclusion

In summary, inspired by biological tactile perception and information processing in neural network, a bionic tactile perceptual platform is proposed. Solution processed PDMS based tactile sensors act as bionic skin touch receptors. While solution processed flexible proton gated indium tin oxide neuromorphic transistors act as artificial synapses. Thus, the tactile perceptual platform possesses the ability of information processing. In addition, in order to ensure the security of information transmission process, an XNOR circuit is adopted to encrypt and decrypt perceptual information. With adoption of cipher, signal transmitted by the perception platform is encrypted. Thus, the security of information transmission is effectively improved. The present work provide an effective strategy for information transmission in bionic tactile perceptual platform with high security. The tactile perceptual platform would have potentials in cognitive wearable devices, advanced human-machine interaction system and intelligent bionic robots.

Acknowledgements

Project supported by the National Natural Science Foundation of China (Grant No. 51972316) and Ningbo Key Scientific and Technological Project (Grant No. 2021Z116).

References

- [1] Zidan M A, Strachan J P and Lu W D 2018 *Nat. Electron.* **1** 22
- [2] Schneider P, Walters W P, Plowright A T, Sieroka N, Listgarten J, Goodnow R A, Fisher J, Jansen J M, Duca J S, Rush T S, Zentgraf M, Hill J E, Krutoholow E, Kohler M, Blaney J, Funatsu K, Luebke C and Schneider G 2019 *Nat. Rev. Drug. Discov.* **19** 353
- [3] Liu X X, Rivera S C, Moher D, Calvert M J and Denniston A K 2019 *Nat. Med.* **26** 1364
- [4] Paek S and Kim N 2021 *Sustainability* **13** 7941
- [5] Schwalbe N and Wahl B 2020 *Lancet* **395** 1579
- [6] Guo Y L, Wang H Y, Hu Q Y, Liu H, Liu L and Bennamoun M 2021 *IEEE Trans. Pattern Anal. Mach. Intell.* **43** 4338
- [7] Song H, Bai J N, Yi Y, Wu J S and Liu L J 2020 *IEEE Comput. Intell. Mag.* **15** 44
- [8] Ullman S 2019 *Science* **363** 692
- [9] Kumar N, Patel M, Nguyen T T, Bhatnagar P and Kim J 2022 *Mater. Today Chem.* **23** 100681
- [10] Zhu J D, Zhang T, Yang Y C and Huang R 2020 *Appl. Phys. Rev.* **7** 011312
- [11] Hu L X, Fu S, Chen Y H, Cao H T, Liang L Y, Zhang H L, Gao J H, Wang J R and Zhuge F 2017 *Adv. Mater.* **29** 1606927
- [12] Huh W, Lee D and Lee C H 2020 *Adv. Mater.* **32** 2002092
- [13] Yan X B, Zhao J H, Liu S, Zhou Z Y, Liu Q, Chen J S and Liu X Y 2018 *Adv. Funct. Mater.* **28** 1705320
- [14] Zhu L Q, Wan C J, Guo L Q, Shi Y and Wan Q 2014 *Nat. Commun.* **5** 3158
- [15] Fu Y, Kong L A, Chen Y, Wang J X, Qian C, Yuan Y B, Sun J, Gao Y L and Wan Q 2018 *ACS Appl. Mater. Interfaces* **10** 26443
- [16] Ge C, Liu C X, Zhou Q L, Zhang Q H, Du J Y, Li J K, Wang C, Gu L, Yang G Z and Jin K J 2019 *Adv. Mater.* **31** 1900379
- [17] Cho S W, Kwon S M, Lee M, Jo J W, Heo J S, Kim Y H, Cho H K and Park S K 2019 *Nano Energy* **66** 104097
- [18] Peng Z H, Wu F C, Jiang L, Cao G S, Jiang B, Cheng G, Ke S W, Chang K C, Li L and Ye C 2021 *Adv. Funct. Mater.* **31** 2107131
- [19] Yang Q, Yang H H, Lv D X, Yu R J, Li E L, He L H, Chen Q Z, Chen H P and Guo T L 2021 *ACS Appl. Mater. Interfaces* **13** 8672
- [20] Sheridan P M, Cai F X, Du C, Ma W, Zhang Z Y and Lu W D 2017 *Nat. Nanotechnol.* **12** 784
- [21] Wang Z Q, Zeng T, Ren Y Y, Lin Y, Xu H Y, Zhao X N, Liu Y C and Ielmini D 2020 *Nat. Commun.* **11** 1510
- [22] Li Y, Xuan Z H, Lu J K, Wang Z R, Zhang X M, Wu Z H, Wang Y Z, Xu H, Dou C M, Kang Y, Liu Q, Lv H B and Shang D S 2021 *Adv. Funct. Mater.* **31** 2100042
- [23] Wan Q, Jiang X Y, Negroiu A M, Lu S G, McKay K S and Abrams T W 2012 *Nat. Neurosci.* **15** 1144
- [24] Stein B E, Stanford T R and Rowland B A 2014 *Nat. Rev. Neurosci.* **15** 520
- [25] Pearson J 2019 *Nat. Rev. Neurosci.* **20** 624
- [26] Tan H W, Tao Q Z, Pande I, Majumdar S, Liu F, Zhou Y F, Persson P O A, Rosen J and Van Dijken S 2020 *Nat. Commun.* **11** 1369
- [27] Ma Y N, Yue Y, Zhang H, Cheng F, Zhao W Q, Rao J Y, Luo S J, Wang J, Jiang X L, Liu Z T, Liu N S and Gao Y H 2018 *ACS Nano* **12** 3209
- [28] Ge G, Zhang Y Z, Shao J J, Wang W J, Si W L, Huang W and Dong X C 2018 *Adv. Funct. Mater.* **28** 1802576
- [29] Yoon S G, Park B J and Chang S T 2017 *ACS Appl. Mater. Interfaces* **9** 36206
- [30] Wu W H, Zhang Q, Zhou X, Li L, Su J W, Wang F K and Zhai T Y 2018 *Nano Energy* **51** 45
- [31] Kim S J, Koh H J, Ren C E, Kwon O, Maleski K, Cho S Y, Anasori B, Kim C K, Choi Y K, Kim J, Gogotsi Y and Jung H T 2018 *ACS Nano* **12** 986
- [32] Fu H R, Zhao Y, Xie T, Han M L, Ma L F and Zang S Q 2018 *J. Mater. Chem. C* **6** 6440
- [33] Yang J C, Mun J, Kwon S Y, Park S, Bao Z N and Park S 2019 *Adv. Mater.* **31** 1904765
- [34] Guo Y, Zhong M J, Fang Z W, Wan P B and Yu G H 2019 *Nano Lett.* **19** 1143
- [35] Peng X, Dong K, Ye C Y, Jiang Y, Zhai S Y, Cheng R W, Liu D, Gao X P, Wang J and Wang Z L 2020 *Sci. Adv.* **6** eaba9624
- [36] Yu Y, Nassar J, Xu C H, Min J H, Yang Y R, Dai A, Doshi R, Huang A, Song Y, Gehlhar R, Ames A D and Gao W 2020 *Sci. Robot.* **5** eaaz7946
- [37] Kim Y, Chortos A, Xu W T, Liu Y X, Oh J Y, Son D, Kang J, Foudeh A M, Zhu C X, Lee Y, Niu S M, Liu J, Pfattner R, Bao Z N and Lee T W 2018 *Science* **360** 998

- [38] Sundaram S, Kellnhofer P, Li Y Z, Zhu J Y, Torralba A and Matusik W 2019 *Nature* **569** 698
- [39] Wang M, Yan Z, Wang T, Cai P Q, Gao S Y, Zeng Y, Wan C J, Wang H, Pan L, Yu J, Pan S W, He K, Lu J and Chen X D 2020 *Nat. Electron.* **3** 563
- [40] Yu J R, Gao G Y, Huang J R, Yang X X, Han J, Zhang H, Chen Y H, Zhao C L, Sun Q J and Wang Z L 2021 *Nat. Commun.* **12** 1581
- [41] Tan H W, Zhou Y F, Tao Q Z, Rosen J and Van Dijken S 2021 *Nat. Commun.* **12** 1120
- [42] Liao X Q, Song W T, Zhang X Y, Yan C Q, Li T L, Ren H L, Liu C Z, Wang Y T and Zheng Y J 2020 *Nat. Commun.* **11** 268
- [43] Tian Y H, Chen X L, Xiong H K, Li H L, Dai L R, Chen J, Xing J L, Chen J, Wu X H, Hu W M, Hu Y, Huang T J and Gao W 2017 *Front. Inform. Tech. El.* **18** 58
- [44] Yu F, Cai J C, Zhu L Q, Sheikhi M, Zeng Y H, Guo W, Ren Z Y, Xiao H, Ye J C, Lin C H, Wong A B and Wu T 2020 *ACS Appl. Mater. Interfaces* **12** 26258
- [45] Abaira V E and Ginty D D 2013 *Neuron* **79** 618